S©MR

СИБИРСКИЕ ЭЛЕКТРОННЫЕ
МАТЕМАТИЧЕСКИЕ ИЗВЕСТИЯ
Siberian Electronic Mathematical Reports
http://semr.math.nsc.ru
ISSN 1813-3304

Том 20, № 2, стр. 144–145 (2023) УДК 519.633.6
https://doi.org/10.33048/semi.2023.20.??? MSC 76T30

HLLC-TYPE METHOD FOR THE BAER-NUNZIATO TYPE MULTIFLUID SYSTEMS

P.A. CHUPROV

Abstract: Paper introduces a HLLC-type solver with approximate contact for the Baer-Nunziato (seven-equation) model, based on a three-wave solver. Method is applicable for problems with strict mechanical equilibrium between phases, like high-speed impacts or laser-induced shock wave processes in metals. Numerical algorithm, based on the introduced method, is tested on different problems, including the 1D simulation of a high-speed metal plates impact. Obtained results show superiority of the modified method over unmodified, especially on relativelly coarse grids.

Keywords: Baer-Nunziato equations, HLLC method, metal plate, high-speed impact, three-fluid model

1 Introduction

The explosion welding process is currently used technology that allows obtaining materials with unique properties. These materials are used in various industries, from the development of armor protection [1] to the construction of thermonuclear reactors [2]. There is a high interest in numerical modeling of these processes due to the impossibility of experimentally tracking

Chuprov, P.A., HLLC-type method for the Baer-Nunziato type multifluid systems.

Работа выполнена в рамках государственного задания 124022400174-3.
Поступила 1 января 2023 г., опубликована 31 декабря 2023 г.

the entire dynamics of the process. Currently, the SPH method has gained significant popularity in modeling these processes, as seen in works such as [3], [4]. Despite its advantages, the SPH method also has some drawbacks, including computational complexity. Another popular approach to modeling explosion welding tasks involves Lagrangian models, particularly the ALE approach, which is presented alongside the SPH method in work [5]. While these methods can excellently model processes within metals, they struggle when simulating gas flow between plates. The ability to simulate gas dynamics during explosion welding on large scales is provided by Eulerian multiphase methods. Among them, one can note models like the ghost-fluid [6] or the Nigmatulin model [7].

In this study, the Baer-Nunziato model will be considered, first introduced in [8], a mathematical model of multiphase media that has gained worldwide recognition for its outstanding mathematical properties, such as hyperbolicity, as well as its wide range of potential applications. However, the issue of its numerical solution remains relevant. Due to its characteristics, the model is often applied to describe fast-moving shock-wave processes, which necessitates the use of Riemann solvers for its resolution. To date, no numerical scheme has been developed that could equally well address the full spectrum of problems investigated using this model. For example, let's examine the solver presented in [9], based on the HLL methodology. This method exhibits excellent numerical stability and is generally very efficient and simple. However, a critical flaw — significant numerical diffusion of volume fraction discontinuities — makes it impossible to apply this numerical method to problems with explicit interfacial boundaries. Another example includes methods based on the HLLC technique, such as [10]. Such methods can accurately convey the state of the contact boundary between substances but are complex to implement, computationally expensive, and importantly, cannot be easily generalized to an arbitrary number of phases. It is worth noting other works, such as [11], [12], which develop certain aspects of numerical solutions for the Baer-Nunziato system of equations and their derivatives.

Within the scope of this study, the work [13] is of particular interest. It describes a method based on the HLLC technique under the assumption of complete mechanical equilibrium of phases, i.e., equality of their velocities and pressures. The numerical method described in the paper shows excellent results in tasks where such assumptions can be made without compromising the depiction of real mechanics. However, as practice applying this method by the author in [14] has shown, there is potential for improvement, the implementation of which is the goal of this work. The ultimate objective of developing this numerical method is to apply it to modeling the problem of high-speed collision of metal plates, similar to what was considered in [14]. Therefore, a three-phase model will be examined in this work.

2 Mathematical model

The three-phase mathematical model is based on the work [8] and is identical to the model discussed in [13]:

$$\mathbf{U}_t + \mathbf{F}_x(u) = \mathbf{H}(\mathbf{U}) + \mathbf{R} \tag{1}$$

$$\mathbf{U} = \begin{bmatrix} \alpha_1 \\ \alpha_1\rho_1 \\ \alpha_1\rho_1 v_1 \\ \alpha_1\rho_1 E_1 \\ \alpha_2 \\ \alpha_2\rho_2 \\ \alpha_2\rho_2 v_2 \\ \alpha_2\rho_2 E_2 \\ \alpha_3\rho_3 \\ \alpha_3\rho_3 v_3 \\ \alpha_3\rho_3 E_3 \end{bmatrix}, \mathbf{F} = \begin{bmatrix} 0 \\ \alpha_1\rho_1 v_1 \\ \alpha_1(\rho_1 v_1^2 + p_1) \\ \alpha v_1(\rho_1 E_1 + p_1) \\ 0 \\ \alpha_2\rho_2 v_2 \\ \alpha_2(\rho_2 v_2^2 + p_2) \\ \alpha_2 v_2(\rho_2 E_2 + p_2) \\ \alpha_3\rho_3 v_3 \\ \alpha_3(\rho_3 v_3^2 + p_3) \\ \alpha v_3(\rho_3 E_3 + p_3) \end{bmatrix}, \mathbf{H} = \begin{bmatrix} -\tilde{v}(\alpha_1)_x \\ 0 \\ \tilde{p}(\alpha_1)_x \\ \tilde{p}\tilde{v}(\alpha_1)_x \\ -\tilde{v}(\alpha_2)_x \\ 0 \\ \tilde{p}(\alpha_2)_x \\ \tilde{p}\tilde{v}(\alpha_2)_x \\ 0 \\ \tilde{p}(\alpha_3)_x \\ \tilde{p}\tilde{u}(\alpha_3)_x \end{bmatrix}, \tag{2}$$

$$\mathbf{R} = \begin{bmatrix} \mu(p_1 - p_3) \\ 0 \\ \lambda(v_3 - v_1) \\ \lambda\tilde{v}(v_3 - v_1) - \mu\tilde{p}(p_1 - p_3) \\ \mu(p_2 - p_3) \\ 0 \\ \lambda(v_3 - v_2) \\ \lambda\tilde{v}(v_3 - v_2) - \mu\tilde{p}(p_3 - p_2) \\ 0 \\ \lambda(v_1 - v_3) \\ \lambda\tilde{v}(v_1 - v_3) - \mu\tilde{p}(p_3 - p_1) \end{bmatrix},$$

$$\alpha_1 + \alpha_2 + \alpha_3 = 1,$$

$$E_k = \frac{v_k^2}{2} + \frac{p_k + \gamma_k P_{0k}}{\rho_k(\gamma_k - 1)} \tag{3}$$

$$\tilde{p} = \sum_{k=1}^{3} \alpha_k p_k, \quad \tilde{v} = \sum_{k=1}^{3} \alpha_k \rho_k v_k / \sum_{k=1}^{3} \alpha_k \rho_k. \tag{4}$$

Here, $\mathbf{U}$ is the vector of conservative variables, $\mathbf{F}$ is the flux vector, $\mathbf{H}(\mathbf{U})$ represents the so-called nozzle terms, and $\mathbf{R}$ is the algebraic source term related to the relaxation of phase pressures and velocities. Standard notations have been used in writing the system of equations: t denotes time, x is the spatial coordinate, α is the volume fraction, ρ is the true density, v is velocity, p is pressure, and E is total energy. The velocity and pressure marked with

tildes correspond to parameters at the interface. Subscripts 1, 2, and 3 refer to the first, second, and third phases, respectively.

This system can easily be generalized to cases involving more phases and higher-dimensional problems. The focus of this study is the development and analysis of a new numerical method, so for simplicity and without loss of generality, the one-dimensional three-phase version of the model presented above will be considered. An example of using the Baer-Nunziato model for two-dimensional simulations can be found in [15], [9], [16].

3 Numerical algorithm

The computational algorithm is based on the Strang splitting scheme. Each time integration step is divided into three substeps: hyperbolic, velocity relaxation, and pressure relaxation. In the context of this work, only the hyperbolic stage is of interest, while algorithms for velocity and pressure relaxation are taken from, for instance, [14]. All subsequent equations belong solely to the hyperbolic step, wherein the influence of the vector $\mathbf{R}$ is disregarded.

In this work, a numerical method for solving the system of differential equations presented in the previous section is proposed. This method is a modification of the method suggested in [13]. The original method relies on the HLLC technique, assuming a three-wave structure for the solution of the elementary Riemann problem for any number and combination of phases. This approach eliminates the need to solve complex nonlinear systems of equations to determine parameters in regions between contact discontinuities of different phases, significantly simplifying the approximation of the spatial derivative of the volume fraction in the compaction equation and in the nozzle terms. Furthermore, this approach can be applied to problems with an arbitrarily large number of phases, which is practically impossible for methods considering more complex wave structures of the Riemann problem's solution. As mentioned earlier, the main drawback of this approach lies in the necessity of mechanical equilibrium between phases, meaning equal speeds and pressures, which does not diminish its value for a specific class of problems.

The wave structure of the three-wave solver is schematically depicted in Fig. 1. The elementary solution consists of just three waves: right, left, and contact discontinuity, regardless of the number of phases involved. The speed of these waves is estimated using the following relations:

$$S^*_{i+1/2} = \frac{\tilde{p}_{i+1} - \tilde{p}_i + \tilde{\rho}_i \tilde{u}_i \left(S^-_{i+1/2} - \tilde{u}_i\right)}{\tilde{\rho}_i \left(S^-_{i+1/2} - \tilde{u}_i\right) - \tilde{\rho}_{i+1} \left(S^+_{i+1/2} - \tilde{u}_{i+1}\right)} - \frac{\tilde{\rho}_{i+1} \tilde{u}_{i+1} \left(S^+_{i+1/2} - \tilde{u}_{i+1}\right)}{\tilde{\rho}_i \left(S^-_{i+1/2} - \tilde{u}_i\right) - \tilde{\rho}_{i+1} \left(S^+_{i+1/2} - \tilde{u}_{i+1}\right)}, \tag{5}$$

$$\tilde{\rho} = \sum_{k=1}^{3} \alpha_k \rho_k, \tag{6}$$

(7)

$$S^+_{i+1/2} = \max_k \{v_{i,k} + c_{i,k}, v_{i+1,k} + c_{i+1,k}\}, \tag{8}$$

$$S^-_{i+1/2} \max_k \{v_{i,k} - c_{i,k}, v_{i+1,k} - c_{i+1,k}\}. \tag{9}$$

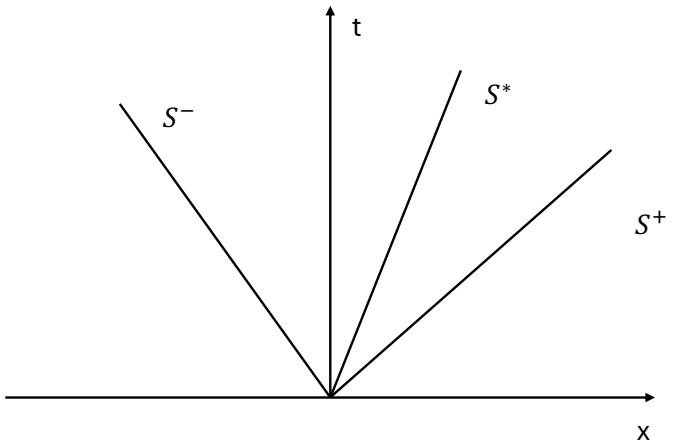

FIG. 1. Wave structure of the three-wave solver

Once all three wave speeds are available, estimates for parameters to the left and right of the contact discontinuity can be obtained using the HLLC method relations:

$$\mathbf{Q}^-_{*,k} = \begin{bmatrix} C^- \\ C^- S^*_{i+1/2} \\ C^- v_{i,k} \\ C^- \left(\frac{p_{i,k}}{\rho_{i,k}} + \left(S^*_{i+1/2} - u_{i,k}\right) \left(S^*_{i+1/2} + \frac{p_{i,k}}{\rho_{i,k} \left(S^-_{i+1/2} - u_{i,k}\right)} \right) \right) \end{bmatrix}, \tag{10}$$

$$C^- = \frac{\alpha_{i,k}\rho_{i,k}\left(S^-_{i+1/2} - u_{i,k}\right)}{\left(S^-_{i+1/2} - S^*_{i+1/2}\right)}, \tag{11}$$

$$\mathbf{Q}^+_* = \begin{bmatrix} C^+ \\ C^+ S^*_{i+1/2} \\ C^+ v_{i+1,k} \\ C^+\left(\frac{p_{i+1,k}}{\rho_{i+1,k}} + \left(S^*_{i+1/2} - u_{i+1,k}\right)\left(S^*_{i+1/2} + \frac{p_{i+1,k}}{\rho_{i+1,k}\left(S^+_{i+1/2} - u_{i+1,k}\right)}\right)\right) \end{bmatrix}, \tag{12}$$

$$C^+ = \frac{\alpha_{i+1,k}\rho_{i+1,k}\left(S^+_{i+1/2} - u_{i+1,k}\right)}{\left(S^+_{i+1/2} - S^*_{i+1/2}\right)}. \tag{13}$$

Here, $\mathbf{Q}^{+,-}_{*,k}$ represents the parameters of phase k to the right and left of the contact discontinuity, respectively.

In the framework of this work, a modified picture of the Riemann problem solution consisting of $2N+1$ waves for a problem with N phases is considered. This wave pattern in the three-phase case is shown in Figure 2.

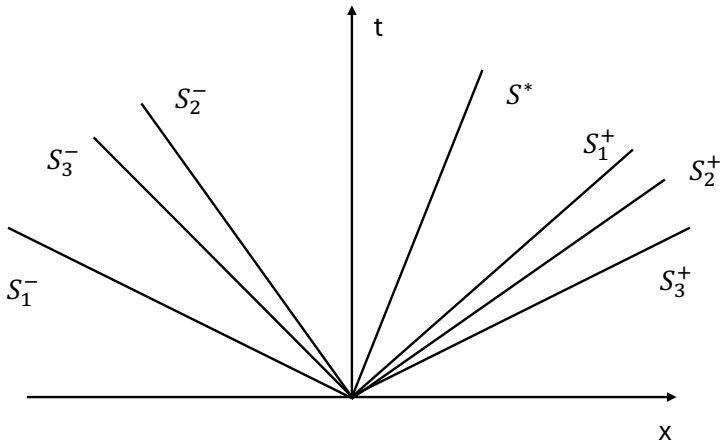

FIG. 2. Wave structure of the proposed multi-wave solver

Unlike the previous case, each phase has its own right and left wave. This refinement does not lead to a complication of the problem's solution. It is known ([12], [10]) that these waves do not interact with each other, being monophasic discontinuities, which allows calculating the parameters behind them independently of the wave configuration of the problem. In the presented wave pattern, only one contact discontinuity is considered, which greatly simplifies the calculation of numerical fluxes across cell interfaces.

However, unlike the method discussed earlier, the following approximation is used for the speed of the contact discontinuity in this work:

$$\tilde{S}^{*}_{i+1/2} = \frac{\tilde{p}_{i+1} - \tilde{p}_i + \tilde{\rho}_i \tilde{u}_i \left(\tilde{S}^{-}_{i+1/2} - \tilde{u}_i\right)}{\tilde{\rho}_i \left(\tilde{S}^{-}_{i+1/2} - \tilde{u}_i\right) - \tilde{\rho}_{i+1} \left(\tilde{S}^{+}_{i+1/2} - \tilde{u}_{i+1}\right)} - \frac{\tilde{\rho}_{i+1} \tilde{u}_{i+1} \left(\tilde{S}^{+}_{i+1/2} - \tilde{u}_{i+1}\right)}{\tilde{\rho}_i \left(\tilde{S}^{-}_{i+1/2} - \tilde{u}_i\right) - \tilde{\rho}_{i+1} \left(\tilde{S}^{+}_{i+1/2} - \tilde{u}_{i+1}\right)}, \tag{14}$$

$$\tilde{S}^{-}_{i+1/2} = \Sigma^{3}_{k=1} \alpha_k S^{-}_{i+1/2,k}, \tag{15}$$

$$\tilde{S}^{+}_{i+1/2} = \Sigma^{3}_{k=1} \alpha_k S^{+}_{i+1/2,k}. \tag{16}$$

Here, the subscript k corresponds to phase number $k = 1 \div 3$. This estimate of the contact discontinuity speed is motivated by the need to correctly describe the case of vanishing phases, where the volume fraction of one or more phases approaches zero. Physically, such phases should not affect the mechanics of the process.

The left and right waves for each phase are approximated as follows:

$$S^{+}_{i+1/2,k} = \max\left\{v_{i,k} + c_{i,k}, v_{i+1,k} + c_{i+1,k}\right\} \tag{17}$$

$$S^{-}_{i+1/2,k} \max\left\{v_{i,k} - c_{i,k}, v_{i+1,k} - c_{i+1,k}\right\} \tag{18}$$

Thus, we can write down the final equations for the parameters to the left and right of the contact discontinuity for each phase:

$$\mathbf{Q}^{-}_{*,k} = \begin{bmatrix} C^{-}_{k} \\ C^{-}_{k} \tilde{S}^{*}_{i+1/2} \\ C^{-}_{k} v_{i,k} \\ C^{-}_{k} \frac{p_{i,k}}{\rho_{i,k}} + C^{-}_{k} \left(\tilde{S}^{*}_{i+1/2} - u_{i,k}\right) \cdot \\ \cdot \left(\tilde{S}^{*}_{i+1/2} + \frac{p_{i,k}}{\rho_{i,k}\left(S^{-}_{i+1/2,k} - u_{i,k}\right)}\right) \end{bmatrix}, \tag{19}$$

$$C^{-}_{k} = \frac{\alpha_{i,k} \rho_{i,k} \left(S^{-}_{i+1/2,k} - u_{i,k}\right)}{\left(S^{-}_{i+1/2,k} - \tilde{S}^{*}_{i+1/2}\right)}, \tag{20}$$

$$\mathbf{Q}^{+}_{*,k} = \begin{bmatrix} C^{+}_{k} \\ C^{+}_{k} \tilde{S}^{*}_{i+1/2} \\ C^{+}_{k} v_{i+1,k} \\ C^{+}_{k} \frac{p_{i+1,k}}{\rho_{i+1,k}} + C^{+}_{k} \left(\tilde{S}^{*}_{i+1/2} - u_{i+1,k}\right) \cdot \\ \cdot \left(\tilde{S}^{*}_{i+1/2} + \frac{p_{i+1,k}}{\rho_{i+1,k}\left(S^{+}_{i+1/2,k} - u_{i+1,k}\right)}\right) \end{bmatrix}, \tag{21}$$

$$C_k^+ = \frac{\alpha_{i+1,k}\rho_{i+1,k}\left(S^+_{i+1/2,k} - u_{i+1,k}\right)}{\left(S^+_{i+1/2,k} - \tilde{S}^*_{i+1/2,k}\right)}. \tag{22}$$

The numerical approximation of the conserved quantities' flux through the cell interface is written as follows:

$$\mathbf{\Phi}_{i+1/2,k} = \begin{cases} \Phi_{i,k}, & \text{if } S^-_{i+1/2,k} \geq 0, \\ \Phi_{i,k} + S^-_{i+1/2,k}\left(\mathbf{Q}^-_{*,k} - \mathbf{W}_{i,k}\right), & \text{if } S^-_{i+1/2,k} < 0, \tilde{S}^*_{i+1/2,k} \geq 0 \\ \Phi_{i+1,k} + S^+_{i+1/2,k}\left(\mathbf{Q}^+_{*,k} - \mathbf{W}_{i+1,k}\right), & \text{if } \tilde{S}^*_{i+1/2} < 0, S^+_{i+1/2,k} \geq 0 \\ \Phi_{i+1,k}, & \text{if } S^+_{i+1/2,k} \leq 0. \end{cases} \tag{23}$$

Here, $\mathbf{\Phi}_{i+1/2,k}$ represents the part of the approximation of the conservative variable flux vector across the interface indexed by $i + 1/2$, corresponding to the phase with index k. $\Phi_{i,k}$ is the portion of the flux vector for the same phase to the left of the interface, and $\mathbf{W}_{i,k}$ is the part of the vector of conservative variables corresponding to the phase with index k:

$$\mathbf{W}_{i,k} = \begin{bmatrix} \alpha_k\rho_k \\ \alpha_k\rho_k v_k \\ \alpha_k\rho_k E_k \end{bmatrix}. \tag{24}$$

The finite-volume scheme for computing these values at the next time step looks as follows:

$$\mathbf{W}_i^{n+1} = \mathbf{W}_i^n - \frac{\Delta t^n}{\Delta x}\left[\mathbf{\Phi}_{i+1/2} - \mathbf{\Phi}_{i-1/2}\right] + \mathbf{H}_i^n. \tag{25}$$

The gradients of the volume fractions in the last term on the right-hand side of Equation 25 are approximated as follows:

$$((\alpha_1)_x)_i^n = \frac{1}{\Delta x}\left((\phi_1)_{i+1/2} - (\phi_1)_{i-1/2}\right), \tag{26}$$

$$((\alpha_2)_x)_i^n = \frac{1}{\Delta x}\left((\phi_2)_{i+1/2} - (\phi_2)_{i-1/2}\right), \tag{27}$$

$$((\alpha_3)_x)_i^n = -((\alpha_1)_x)_i^n - ((\alpha_2)_x)_i^n, \tag{28}$$

$$(\phi_1)_{i+1/2} = \begin{cases} (\alpha_1)_i^n, \text{ if } (\tilde{S}^*_{i+1/2} \geq 0, \\ (\alpha_1)_{i+1}^n, \text{ else }. \end{cases}, \tag{29}$$

$$(\phi_2)_{i+1/2} = \begin{cases} (\alpha_2)_i^n, \text{ if } \tilde{S}^*_{i+1/2} \geq 0, \\ (\alpha_2)_{i+1}^n, \text{ else }. \end{cases}. \tag{30}$$

The first and fifth equations of system 2, describing the transport of the volume fraction of the first and second phases, respectively, are approximated as follows:

$$(\alpha_1)_i^{n+1} = (\alpha_1)_i^n - \Delta t \tilde{v}_i^n ((\alpha_1)_x)_i^n, \tag{31}$$

$$(\alpha_2)_i^{n+1} = (\alpha_2)_i^n - \Delta t \tilde{v}_i^n ((\alpha_2)_x)_i^n. \tag{32}$$

Similarly to the original method, often called "three-wave solver", in the current work the proposed above method will be called "multi-wave solver" for simplicity.

4 Test problems

4.1. Two-phase gas shock tube. A shock tube problem containing two different gases is considered. At the initial moment, one gas occupies the left part of the tube, while another gas fills the right part. Both gases are assumed to be ideal, meaning they follow the equation of state given by $p = (\gamma - 1)\rho e$. The length of the tube is 1 meter, and initially, the boundary between the gases is located exactly halfway, at 0.5 meters. The initial conditions of the problem are shown in Figure 3.

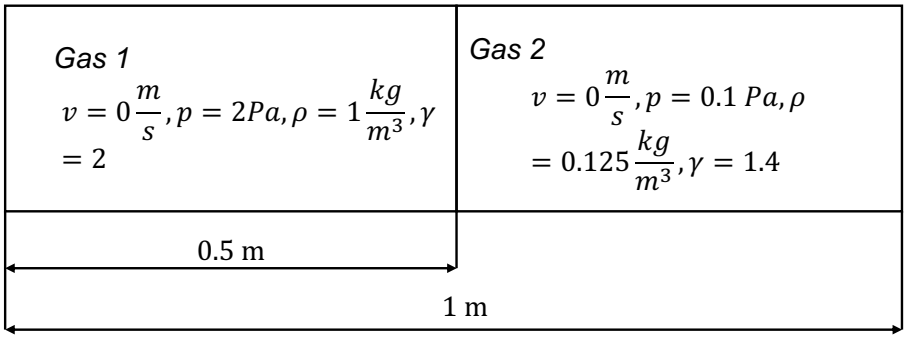

FIG. 3. Schematic statement of the two-gas schock tube problem

It is important to note that this problem is a two-phase one, whereas the mathematical model and computational method explicitly assume the presence of three phases in the computational domain. This fact does not hinder simulation. In the calculations presented here and later, the parameters of the equation of state for the first phase correspond to the first gas, while the second and third phases correspond to the second gas. Thus, the second and third phases each occupy half of the volume allocated to the second gas according to the problem statement. It is also crucial to mention that the mathematical model does not allow the volume fraction of any phase to become zero. Therefore, in areas where, according to the problem setup, only one gas is present, its volume fraction is set to $1 - 10^{-5}$. This value has been determined empirically and ensures optimal algorithm stability.

To confirm mesh convergence, computations were performed with varying numbers of cells, $N = 50, 100, 200,$

500, 1000. The results of the second order accurate Godunov solver computation with $N_{cells} = 1000$ are also included for comparison. The results are displayed in Figure 4.

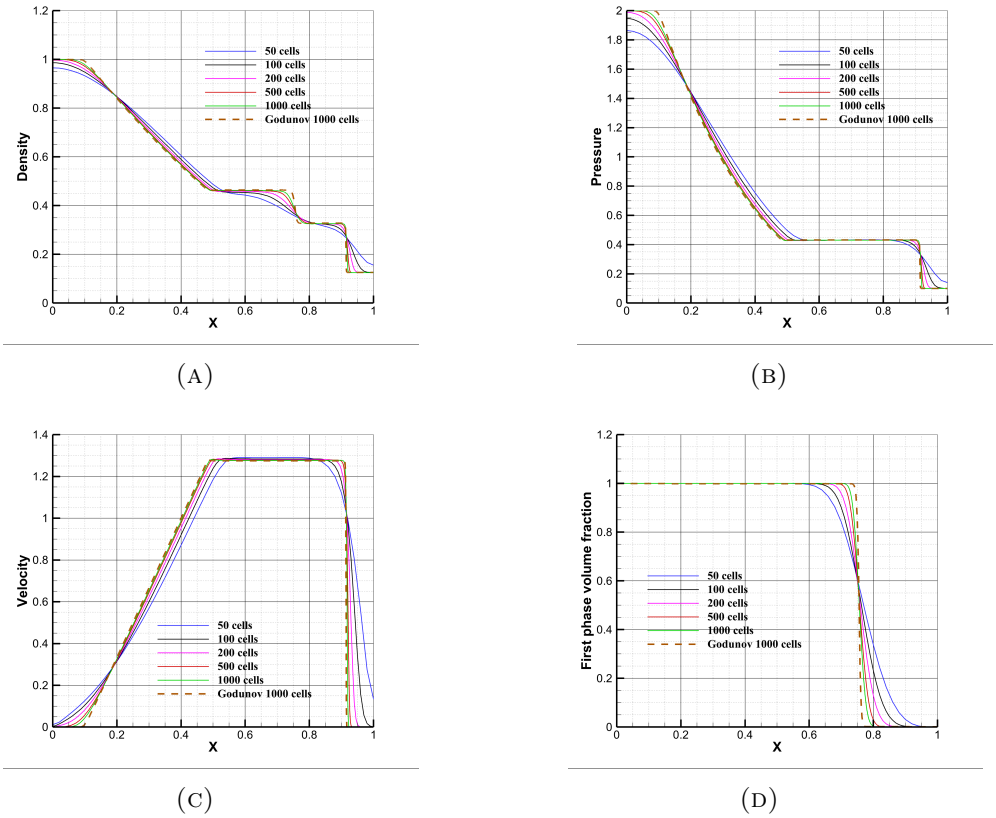

FIG. 4. Spatial distributions of key variables at time $t = 0.2$ s. From left to right, top to bottom: density, pressure, velocity, volume fraction of the first phase.

The differences between the presented method and the original method from [13] on meshes with $N = 100$ and $N = 1000$ cells are presented in Figures 5 and 6, respectively. The results obtained with the presented method on a coarse grid consisting of 100 cells clearly show less numerical dissipation. For example, in Figure 5b, this effect is evident on the inclined region corresponding to the rarefaction wave. Meanwhile, in the area of the shock wave and at the interface between phases, the difference between the methods is almost imperceptible, as seen, for instance, in Figure 5d.

Results obtained on a finer grid demonstrate similar behavior, with improved resolution in the rarefaction wave region and an expected decrease in the difference between the results of different methods due to a tenfold increase in the number of cells.

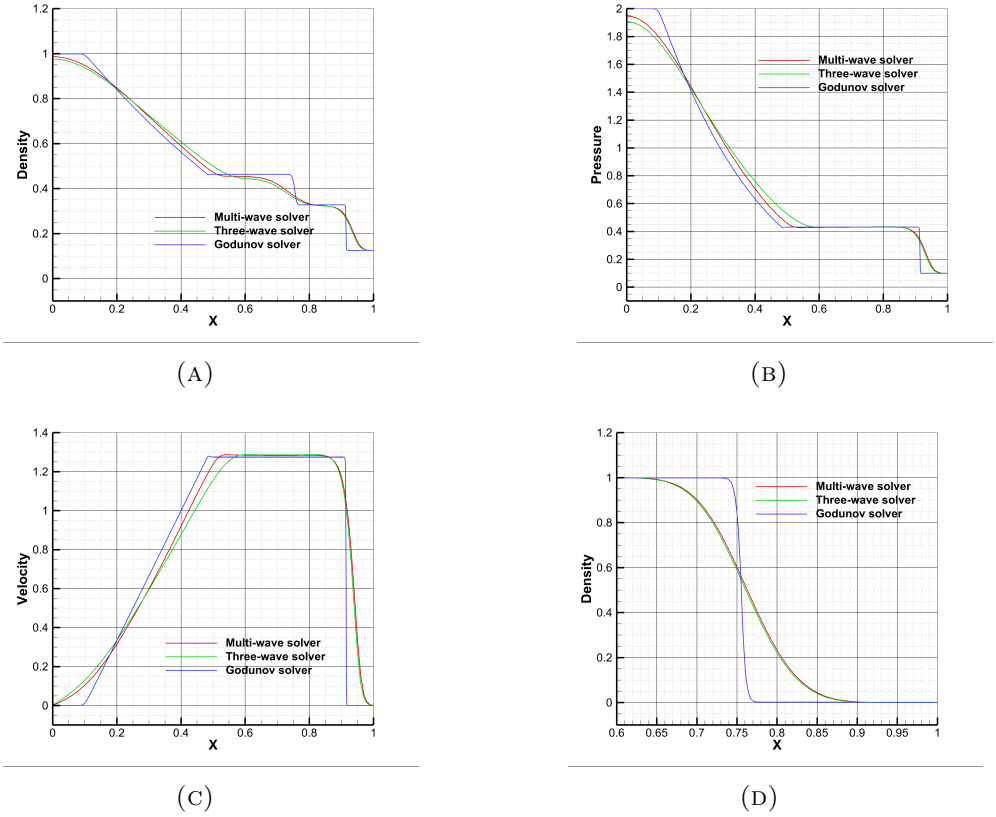

FIG. 5. Spatial distributions of variables at time 0.2 seconds comparing different numerical methods on a grid with 100 cells. Left to right, top to bottom: density, pressure, velocity, volume fraction of the first phase. Red lines represent the modified method, green lines represent the original method, blue lines are the results of the second order Godunov solver.

4.2. Gas-fluid shock tube. The problem analogous to the one presented in the previous section is considered, but with notable complication. One of the gases is replaced by a fluid with a two-equation state corresponding to water. Thus, the problem consists of a shock tube divided into two chambers at the initial moment. On the left is pressurized water, and on the right is pure air under normal conditions. The problem setup is taken from [9] and [17], where it was also used to verify developed numerical methods. It is worth mentioning that this test is quite challenging and designed to check the stability of the developed method. The initial parameters of the problem are shown in Figure 7.

The transformation of the two-phase physical setup was carried out similarly to the previous problem.

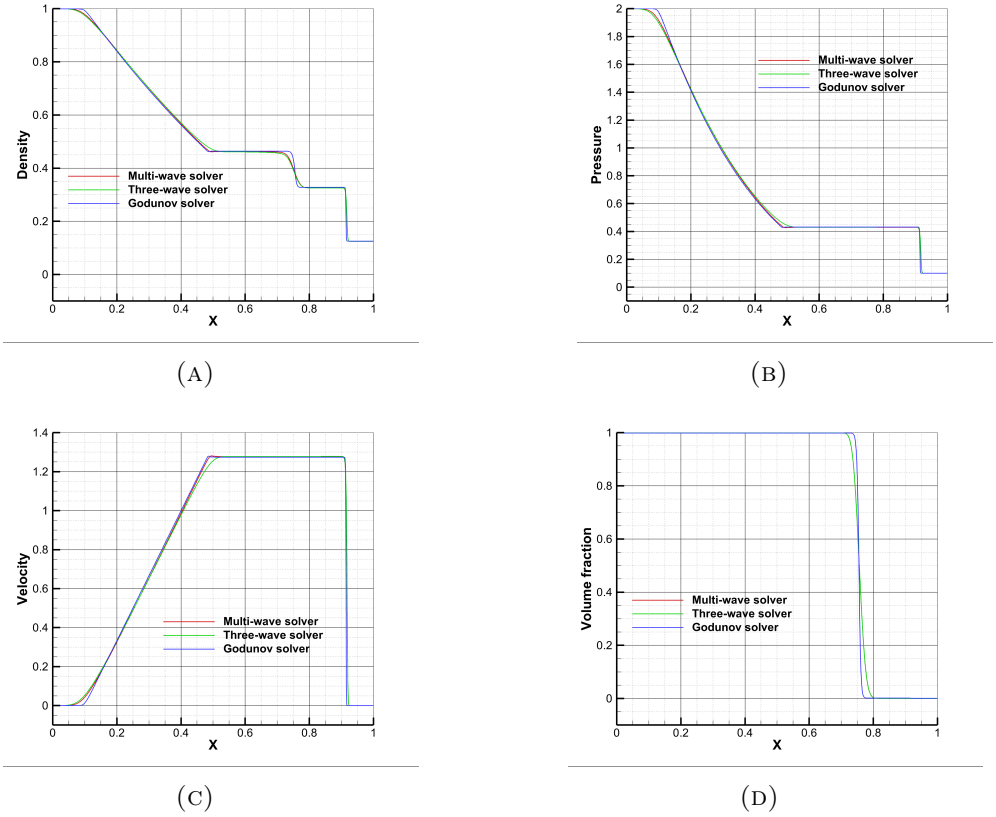

FIG. 6. Spatial distributions of variables at time 0.2 seconds comparing different numerical methods on a grid with 1000 cells. Left to right, top to bottom: density, pressure, velocity, volume fraction of the first phase. Red lines represent the modified method, green lines represent the original method, blue lines are the results of the second order Godunov solver.

Figure 8 presents the results of the mesh convergence study for the simulation of the described problem using the presented method alongside with the analytical solution of the problem. The results indicate the existence of mesh convergence consistent with the first-order approximation of the used numerical method. No unphysical oscillations or artifacts are observed in the results.

As with the investigation of the previous test problem, the methods were compared on grids with $N = 100$ and $N = 1000$ cells. The results are shown in Figures 9 and 10, respectively.

The presented results, as before, show good agreement between the methods, with the advantage of the modified method in resolving wave fronts. This is especially noticeable in Figure 9c, where the leading edge of the wave exhibits

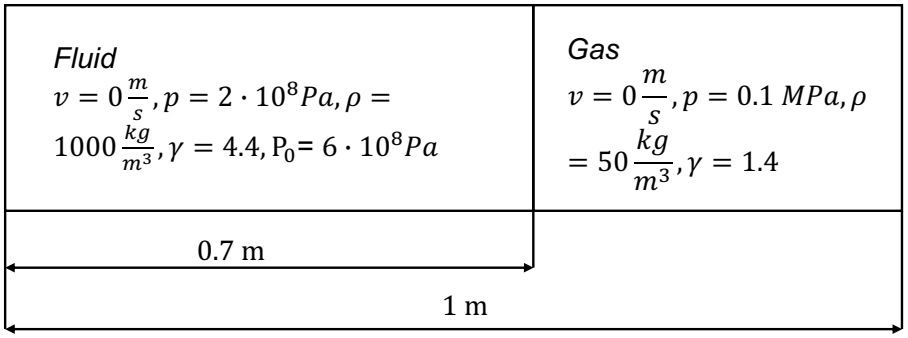

FIG. 7. Schematic statement of the gas-fluid shock tube problem

significantly lower numerical dissipation in the results obtained using the modified method. Increasing the number of cells does not qualitatively alter the conclusions already drawn.

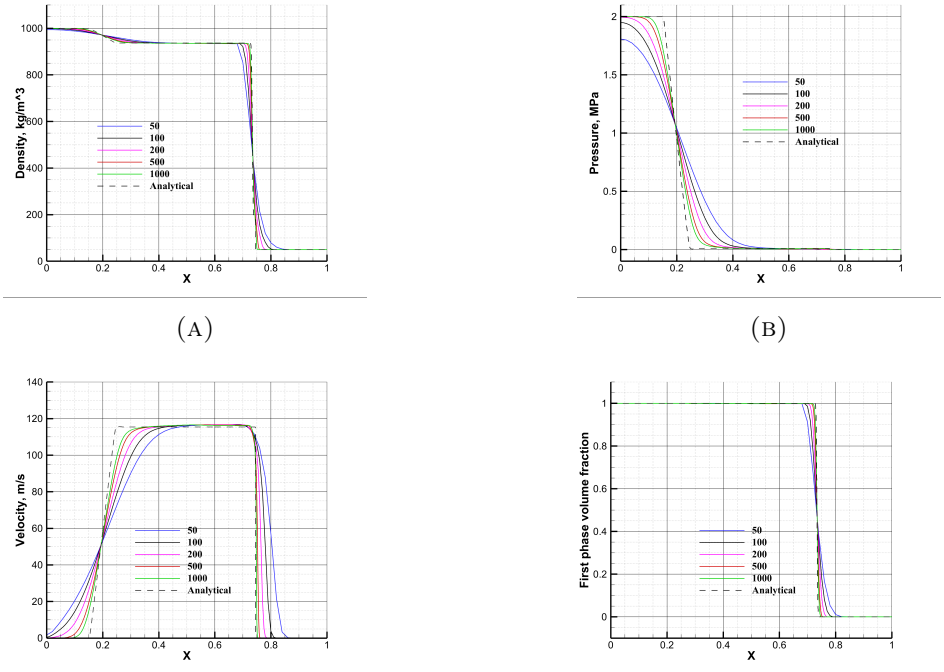

(A) (B)

(C) (D)

FIG. 8. Spatial distributions of variables at the time instant of 0.291 ms. From left to right, top to bottom: density, pressure, velocity, volume fraction of the first phase.

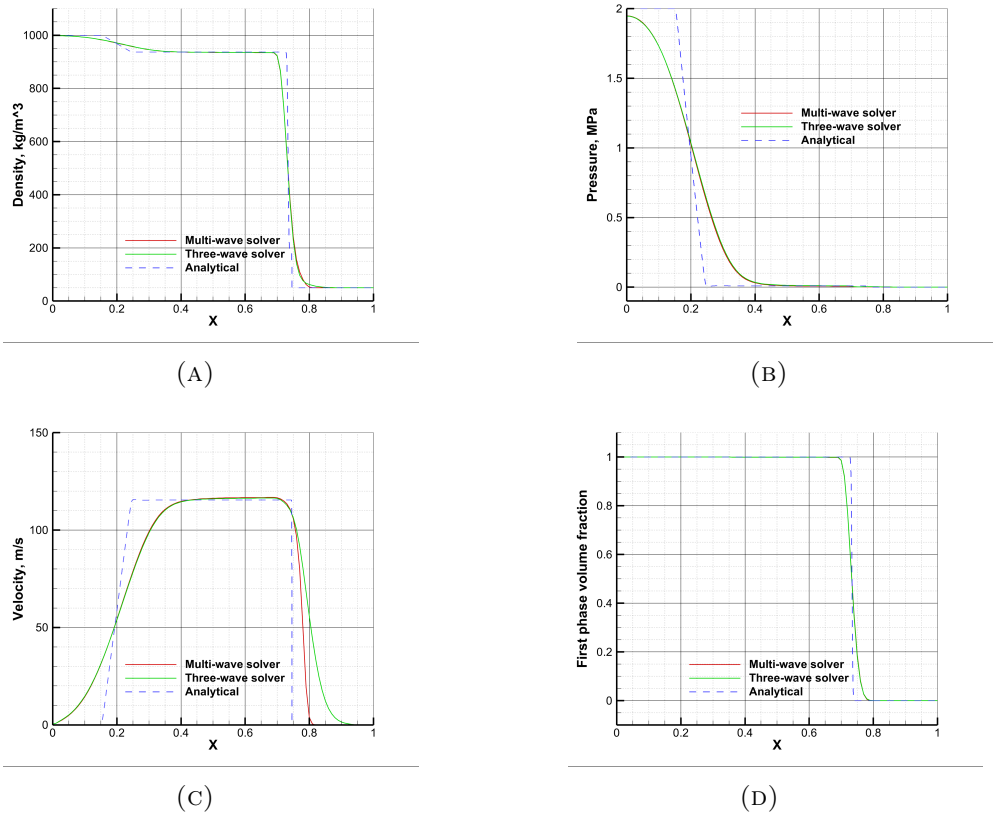

FIG. 9. Spatial distributions of variables at the time instant of 0.291 ms comparing different numerical methods on a grid with 100 cells. Left to right, top to bottom: density, pressure, velocity, volume fraction of the first phase.

5 High-speed metal plates impact

To demonstrate the advantages of the modifications made to the method, the classic problem of high-speed collision of metallic plates is considered. Examples of numerical simulations of such problems can be found in the works of S.K. Godunov, for instance, in [18] or [19]. In this work, we will analyze the problem setup from [14], which consists of four regions, each containing three phases: air, steel, and lead. We will consider a one-dimensional approximation of the process. Initially, the lead plate is in contact with the steel plate and moves towards it as a single unit at a speed of 500 m/s. As shown in [20], during the initial stages of this process metals behave like a weakly compressible fluids. This period lasts roughly for the first 10 μs from the initial contact. A schematic representation of the problem setup is shown in Figure 11.

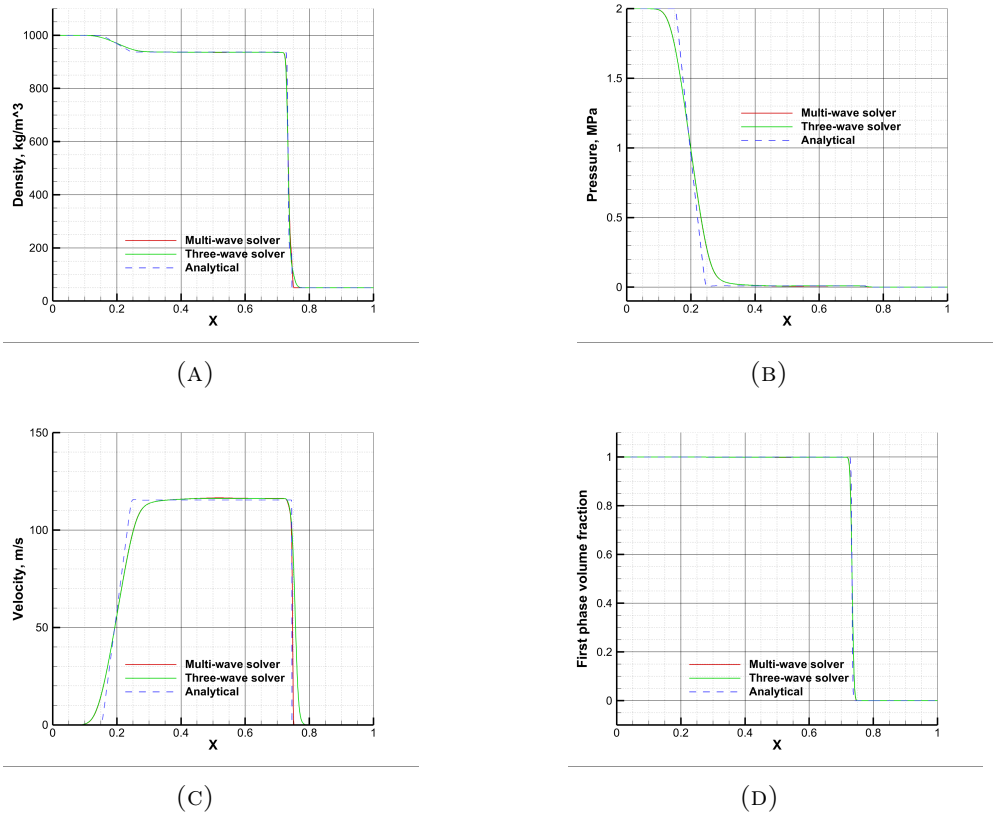

FIG. 10. Spatial distributions of variables at the time instant of 0.291 ms comparing different numerical methods on a grid with 1000 cells. Left to right, top to bottom: density, pressure, velocity, volume fraction of the first phase.

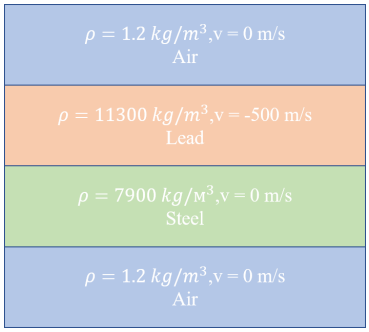

FIG. 11. Schematic statement of the metal plates impact problem

Two computational grids with cell counts $N1 = 180$ and $N2 = 1800$ are introduced. Figure 12 displays the results of calculations on these grids using both methods at times 0.13, 0.26, and 0.39 milliseconds.

The results obtained on the coarse grid exhibit the greatest discrepancy between methods. Figure 12a shows that the results produced by the unmodified method contain non-physical oscillations absent in the modified method's results. Importantly, these oscillations occur specifically at the contact boundary between different materials. The subsequent evolution of the solution on the coarse grid reveals that these oscillations do not completely disappear and continue to influence the numerical solution, as seen in Figures 12c and 12e. In contrast, the modified method demonstrates a complete absence of any non-physical artifacts and a lower level of numerical dissipation at the shock wave front.

The results obtained on the fine grid reveal smaller differences between the solvers. On the fine grid, both methods produce physically accurate solutions without artifacts or oscillations. Nevertheless, even here, the advantage of the modified method in resolving the shock wave front becomes apparent, particularly when examining the rightward-propagating shock wave.

As one can see from the tests above, the main advantage of the multi-wave solver is the sharper resolution of the SW and RW near contact between phases. This advantage comes from the better approximation of the signal velocities and fluxes in mixed cells in the multi-wave solver. As we move away from the phase contact the influence of the mixed cells decreases, and the solutions converge to each other. This is also the reason why the difference is bigger on the coarser grids. The same number of the mixed cells occupy more space, producing errors.

6 Conclusion

This work introduces a modification to a numerical method for solving differential equation systems that describe the dynamics of multiphase media. The method is based on the HLLC approach and successfully models processes equilibrated in velocity and pressure, outperforming the original variation upon which it is founded. The results obtained in this study highlight a substantial advantage in resolving wave fronts and contact boundaries, as well as the absence of non-physical solution artifacts, particularly when working with relatively coarse grids, which can be beneficial for conserving computational resources.

The demonstrated benefits of the modified method stem directly from considering a more comprehensive wave structure of the process. Employing physically correct signal speed estimates for each phase and modifying the estimation of the contact discontinuity speed yields a more precise and stable method.

For the future research, the main goal is to implement this method in a 2D and 3D geometries. This will allow for the study of the multidimensional problems related to the explosion welding process.

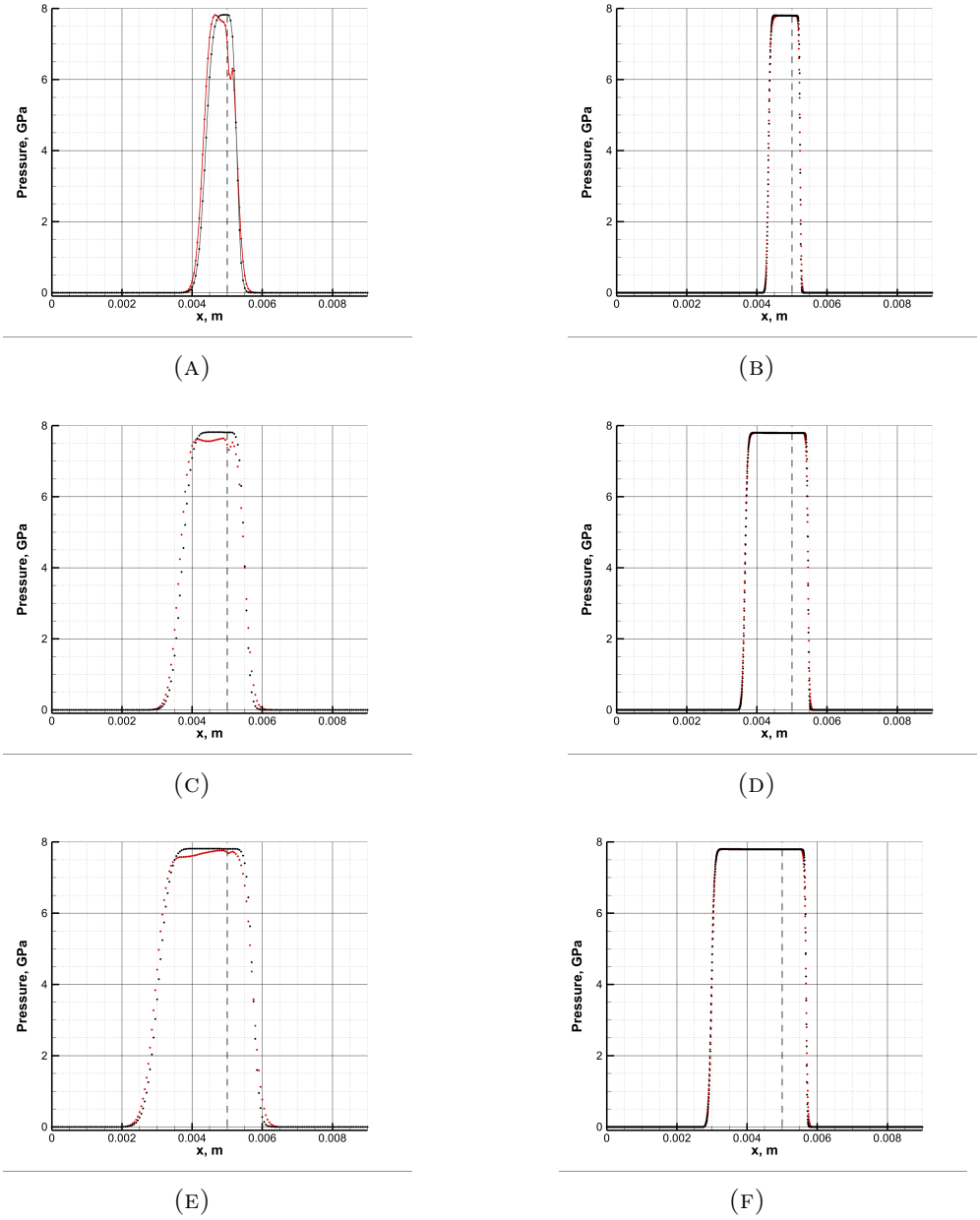

FIG. 12. Spatial pressure distributions at times 0.13, 0.26, and 0.39 milliseconds. The left column shows results on the coarse grid with $N = 180$, and the right column shows results on the fine grid with $N = 1800$. Black lines correspond to results obtained using the presented method, red lines correspond to the method from [13]. The dotted line indicates the initial position of the interface between the plates.

References

[1] D. Krukov, *Promising lightweight crack-resistant armor obtained using technology explosion welding technology*, Strengthening Technologies and Coatings, **10** (2022), 440—443.

[2] E. Carton, M. Stuivinga, *Explosive Cladding for ITER Components*,Materials Science Forum, **566** (2007), 149–154

[3] M. Liu, Z. Zhang, D. Feng, *A density-adaptive SPH method with kernel gradient correction for modeling explosive welding*, Computational Mechanics, **60** (2017), 513-529

[4] Q. Zhou, J. Feng, P. Chen, *Numerical and Experimental Studies on the Explosive Welding of Tungsten Foil to Copper*, Materials, **10** (2017)

[5] A. Nassiri, B. Kinse, *Numerical studies on high-velocity impact welding: smoothed particle hydrodynamics (SPH) and arbitrary Lagrangian-Eulerian (ALE)*, Journal Of Manufacturing Processes, **24** (2016), 376–381

[6] R. Fedkiw, T. Aslam, B. Merriman, S. Osher, *A Non-oscillatory Eulerian Approach to Interfaces in Multimaterial Flows (the Ghost Fluid Method)*, Journal Of Computational Physics, **152** (1999), 457–492

[7] R. I. Nigmatulin, *Equations of fluid mechanics and compaction waves in a two-speed and two-temperature continuous medium in the presence of phase transformations*, Fluid Dynamics, (1967), 33–47

[8] M. Baer, J. Nunziato, *A two-phase mixture theory for the deflagration-to-detonation transition (ddt) in reactive granular materials*, International Journal Of Multiphase Flow, **12** (1986), 861–889

[9] R. Saurel, O. Lemetayer, *A multiphase model for compressible flows with interfaces, shocks, detonation waves and cavitation*, Journal Of Fluid Mechanics, **431** (2001), 239–271

[10] S. Tokareva, E. Toro, *HLLC-type Riemann solver for the Baer–Nunziato equations of compressible two-phase flow*, Journal Of Computational Physics, **229** (2010), 3573–3604

[11] D. Furfaro, R. Saurel, *A simple HLLC-type Riemann solver for compressible non-equilibrium two-phase flows*, Computers & Fluids, **111** (2015), 159–178

[12] H. Lochon, F. Daude, P. Galon J. Hérard, *HLLC-type Riemann solver with approximated two-phase contact for the computation of the Baer–Nunziato two-fluid model* Journal Of Computational Physics, **326** (2016), 733–762

[13] S. Liang, W. Liu, L. Yuan, *Solving seven-equation model for compressible two-phase flow using multiple GPUs*, Computers & Fluids, **99** (2014), 156–171

[14] P. Chuprov, P. Utkin, S. Fortova, *Numerical Simulation of a High-Speed Impact of Metal Plates Using a Three-Fluid Model*, Metals, **11** (2021)

[15] Y. Sugiyama, T. Homae, T. Matsumura, K. Wakabayashi, *Numerical study on the mitigation effect of glass particles filling a partially confined space on a blast wave*, International Journal Of Multiphase Flow, **136** (2020), 103546

[16] P. Utkin, P. Chuprov, *Numerical simulation of shock wave propagation over a dense particle layer using the Baer–Nunziato model*, Physics Of Fluids, **35** (2023), 113313

[17] V. Dobrev, T. Kolev, R. Rieben, V. Tomov, *Multi-material closure model for high-order finite element Lagrangian hydrodynamics*, International Journal For Numerical Methods In Fluids, **82** (2016), 689–706

[18] S. Godunov, A. Deribas, A. Zabrodin, N. Kozin, *Hydrodynamic effects in colliding solids* Journal Of Computational Physics, **5** (1970), 517–539

[19] S. Godunov, S. Kiselev, I. Kulikov, V. Mali, *Numerical and experimental simulation of wave formation during explosion welding*, Proceedings of the Steklov Institute of Mathematics, **281** pp. 12-26 (2013)

[20] I. Yakovlev. *Instability of the interface between colliding metals*, Combustion, Explosion And Shock Waves, **9** (1973), 390–393

Petr Anatolievich Chuprov
Institute for Computer Aided Design,
ul. 19/18 2nd Brest Street,
Moscow, 123056, Russian Federation
Email address: petchu@mail.ru